



Chromophoric dissolved organic matter (CDOM) source characterization in the Louisiana Bight

Robert F. Chen^{a,*}, Paul Bissett^b, Paula Coble^c, Robyn Conmy^c, G. Bernard Gardner^a, Mary Ann Moran^d, Xuchen Wang^a, Mark L. Wells^e, Paul Whelan^a, Richard G. Zepp^f

^a*Environmental, Coastal and Ocean Sciences, University of Massachusetts Boston, 100 Morrissey Boulevard, Boston, MA 02125-3393, USA*

^b*Florida Environmental Research Institute, 4807 Bayshore Boulevard, Suite 101, Tampa, FL 33611, USA*

^c*College of Marine Sciences, University of South Florida, St. Petersburg, FL 33701, USA*

^d*Department of Marine Sciences, University of Georgia, Athens, GA 30602, USA*

^e*School of Marine Science, University of Maine, Orono, ME 04469 USA*

^f*U.S. Environmental Protection Agency, 960 College Station Road, Athens, GA 30605, USA*

Received in revised form 9 March 2004; accepted 9 March 2004

Abstract

Chromophoric dissolved organic matter (CDOM) in the Mississippi plume region may have several distinct sources: riverine (terrestrial soils), wetland (terrestrial plants), biological production (phytoplankton, zooplankton, microbial), and sediments. Complex mixing, photodegradation, and biological processes make differentiation of the specific sources of CDOM difficult. Using a combination of high resolution in situ observations on an undulating vehicle, the ECOShuttle, a pumping system mounted on the vehicle, and detailed chemical and biological analyses of discrete samples allowed us to characterize two specific sources of CDOM in the Louisiana Bight: the river water constrained in the upper 12 m of the Mississippi River plume and several subsurface layers of CDOM below the plume. The subsurface CDOM maxima were coincident with steep pycnoclines and sometimes with maxima in chlorophyll *a* fluorescence. Both sources were actively supplying CDOM to the same location by entirely different processes. The subsurface CDOM was more biologically labile and photochemically refractory than the surface CDOM. Optical properties were also different with a relatively higher protein fluorescence and a lower spectral slope coefficient in the subsurface CDOM. The geographical extent of the two sources was determined by three-dimensional mapping of the area, and due to the relatively calm conditions in the summer of 2000, thin layers of CDOM produced in the subsurface were observed throughout the region. While riverine inputs dominated the distribution of CDOM in surface waters <12 m in depth, biological production of CDOM, probably due to the bacterial degradation of phytoplankton produced DOM dominated the subsurface waters.

© 2004 Elsevier B.V. All rights reserved.

Keywords: Chromophoric dissolved organic matter; Source characterization; Louisiana Bight

* Corresponding author. Tel.: +1-617-287-7491; fax: +1-617-287-7474.

E-mail address: bob.chem@umb.edu (R.F. Chen).

1. Introduction

Chromophoric dissolved organic matter (CDOM) is an easily measured fraction of the total dissolved organic matter that affects remote sensing of surface waters, water column light penetration, and photochemical processes (Chen, 1999; Bissett et al., 2001a,b; Blough and Del Vecchio, 2002; Zepp, 2002). In coastal areas, many possible sources of CDOM, such as rivers, sewage, phytoplankton, zooplankton, bacteria, and sediments, may contribute to the overall CDOM concentration in the water column, while several processes such as mixing, photodegradation, biodegradation, and flocculation affect CDOM distributions. Rivers have dominated the source of CDOM in some coastal systems (DeGrandpre et al., 1996; Del Castillo et al., 1999; Rochelle-Newall and Fisher, 2002a) while in situ production of CDOM has been shown to be more significant than riverine inputs in a shelf-wide budget of CDOM in the Mid-Atlantic Bight (Chen et al., 2002). Zooplankton may produce CDOM during sloppy feeding or by producing leaky fecal pellets (Urban-Rich, 1999). Thin layers of CDOM in East Sound (WA) have been observed where excess CDOM (above what would be expected from mixing of riverine and marine waters) was correlated with oxygen supersaturation suggesting a rapid, direct link between primary production and CDOM production (Twardowsky and Donaghay, 2001). However, phytoplankton have been shown to produce little CDOM directly while bacteria have been shown to convert fresh phytoplankton detritus into CDOM (Nelson et al., 1998; Rochelle-Newall et al., 1999; Rochelle-Newall and Fisher, 2002b). Fluorescent DOM (FDOM) has been shown to be produced as particles degrade in the water column, presumably by bacterial degradation in correlation with the regeneration of nutrients in mid-depth waters (Hayase et al., 1988; Chen and Bada, 1992; Hayase and Shinozuka, 1995). Diffusion of sediment porewaters that are high in CDOM have been shown to affect water column distribution in specific areas (Chen and Bada, 1989; Skoog et al., 1996; Burdige et al., 1999).

Given these multiple sources and complex mixing processes in estuaries and coastal oceans, it has proven difficult to definitively separate these various sources of CDOM (Twardowsky and Donaghay,

2001). Several optical and chemical analyses have been used to attempt to characterize the various source endmembers. Excitation-Emission Matrix (EEM) spectrofluorometry has been used to differentiate marine from terrestrial endmember FDOM (Coble, 1996; De Souza Sierra et al., 1994, 1997). The wavelength of maximum emission is generally shifted to higher wavelengths for terrestrially derived material. The exponentially decaying absorption with wavelength appears to have a steeper log-linearized slope for blue water or photodegraded water compared with riverine sources (Blough and Del Vecchio, 2002). The presence and concentration of lignin phenols has been used as a biomarker of terrestrially derived OM in the ocean (Meyers-Schulte and Hedges, 1986; Opsahl and Benner, 1997). Bioassays such as the concentration of biologically labile photoproducts have been used to assess the quality of the CDOM that is present and as such may indicate source (Moran and Zepp, 1997, 2000).

Additionally, the availability of high resolution techniques to observe CDOM in coastal oceans has increased dramatically in recent years with the advent of small, commercially available CDOM fluorimeters that can be mounted on moorings or towed vehicles (Chen, 1999; Chen and Gardner, 2004, this issue). This paper describes a combination of high resolution, in situ measurements, a continuous pumping system to allow guided sampling, and more detailed characterization methods that show clear differentiation of two sources of CDOM within the same water column.

2. Methods

2.1. Study site

The Mississippi River plume was investigated from June 21–28, 2000 on the RV Pelican. The overall cruise track, scientific objectives, and regional results are discussed elsewhere (Chen and Gardner, 2004, this issue). The ECOShuttle was towed on transects crossing the Mississippi River plume on both the westside and the eastside of the Birdfoot Region. Investigations of the water column were limited to the upper 40 m due to the capability of the ECOShuttle and the main features of interest.

2.2. ECOShuttle

The ECOShuttle is a towed, undulating vehicle based on the Nu-Shuttle (Chelsea Instruments) and has temperature, conductivity, depth, altitude, dissolved oxygen, optical backscatter, CDOM fluorescence, and chlorophyll fluorescence sensors mounted on it to provide real-time, in situ measurements of key water column parameters (Chen and Gardner, 2004, this issue). The ECOShuttle normally operates in a sawtooth undulation pattern from 3 to 45 m depth at a tow speed of ~ 8 knots. In addition, it carries a 4 in. diameter stainless steel pump that forces clean seawater through the 200 m \times 1/2 in. ID Teflon tube incorporated in the tow cable to the ship's laboratory. This flowing seawater passes through a Wetlabs AC-9 absorption meter and a Wetlabs SAFire spectrofluorometer. By carefully determining the transit times of water entering the pump to that exiting the sampling port (~ 3 min), samples can be collected from oceanographic features measured by the in situ instrumentation mounted on the ECOShuttle.

2.3. AC-9

A Wetlabs AC-9 was mounted in the shipboard laboratory. Uncontaminated, unfiltered seawater from the ECOShuttle pumping system was continuously pumped through both the A (absorption) and C (attenuation) flow cells. The AC-9 collects absorption/attenuation intensities at 9 wavelengths from 412 to 750 nm. Generally CDOM was recorded as the absorption at 412 nm (the lowest wavelength available) in the A cell (reflective sides of this flow cell transmit scattered light for the most part so losses in the tube are due solely to absorption). Milli-Q water was used as a reference. The AC-9 measurements at 750 nm were used to correct for scattering (Babin and Stramski, 2002).

2.4. Discrete samples

Discrete samples pumped from the surface as well as subsurface CDOM maxima (16–30 m) were collected and analyzed by a variety of methods. DOC, fluorescence, and absorbance samples were filtered through precombusted (4 hours at 500 °C) glass fiber filters (0.7 μ m) and stored (acidified and

refrigerated for DOC, frozen for fluorescence and absorbance) until analysis. Fluorescence was measured on a Photon Technologies International QM-1 spectrofluorometer with $\lambda_{\text{ex}}=337$ nm calibrated to quinine sulfate units (Chen and Gardner, 2004, this issue). All slits widths were set to 4 nm. Emission spectra were integrated from 350 to 600 nm. Spectra were blank subtracted (to remove the water Raman scattering peak). CDOM fluorescence is expressed as quinine sulfate units (QSU) where 1 QSU is equivalent to the fluorescence emission of 1 μ g/l quinine sulfate solution.

Absorbance measurements (190–800 nm) were made with a Cary 50 spectrophotometer in a 10 cm pathlength cell (Chen and Gardner, 2004, this issue) after thawed samples were re-filtered through 0.45 polycarbonate filters. Milli-Q water was used as a reference and spectra were baseline corrected by subtracting 700–800 nm values from the entire spectrum.

Dissolved organic carbon was measured by high temperature combustion (Vlahos et al., 2002). Briefly, 50 μ l injections of sparged, acidified seawater were combusted at 800 °C and the resultant CO₂ was purified and measured with a Li-COR NDIR detector. Both response factors and blanks were compared with intercomparison standards provided by J. Sharp (U. Delaware) and D. Hansell (U. Miami).

2.5. Excitation–emission matrix (EEM) spectrofluorometry

An ISA-SPEX Fluorolog 3–12 spectrofluorometer was used to measure EEMs of discrete samples after filtration (0.2 μ m). Details of this procedure are provided elsewhere (Zepp et al., 2004, this issue). Basically, emission scans (2 nm resolution) were taken for varying excitation wavelengths (every 5 nm). A new “excision, interpolation” technique was used to eliminate Rayleigh and Raman scattering peaks, and EEMs were normalized to quinine sulfate (Zepp et al., 2004, this issue).

2.6. Biological reactivity

The susceptibility of the surface and subsurface DOM layers to degradation by natural microbial communities was measured by respiration bioassays.

Filtered (0.2 μm) samples were dispensed into glass BOD bottles, inoculated with a ‘standard’ inoculum (i.e., the same inoculum was used for all the experiments), and supplemented with inorganic nutrients. Three replicates of each treatment (subsurface or surface) were fixed with Winkler chemicals for $T=0$ oxygen concentrations; three other replicates were incubated for two weeks and then fixed. All samples were titrated at the same time with an automatic Mettler titrator.

2.7. Photochemical reactivity

Filtered (0.2 μm) surface and subsurface DOM samples were placed in quartz tubes and irradiated in an Atlas Suntest CPS solar simulator for 4 h. The irradiance in this system is approximately equivalent to that received on a clear day at the ocean surface, latitude 30°N during mid-July. Subsamples were collected for optical analyses before and after irradiation. The remainder was dispensed into BOD bottles and analyzed for biological reactivity as described above.

2.8. Optical measurements for biological and photochemical reactivity

All spectra for these experiments were obtained using using 0.2 μm filtered samples. UV–visible absorbances were measured before and after irradiation using an Agilent Model 8453 UV–Visible System (Zepp et al., 2004, this issue). After correcting these spectra by subtracting the average absorbance in the 675–725 nm region, absorption coefficients were computed. Non-linear exponential regression over the wavelength range of 280–400 nm was applied to the absorption coefficients to compute spectral slope coefficients (S). The exponential fit to the data for the subsurface maxima CDOM ($r^2 > 0.96$) was generally somewhat poorer than for the plume (surface) CDOM ($r^2 > 0.99$). Fluorescence spectra (EEMs) were measured as described above before and after irradiation.

2.9. In situ optical modeling and satellite data

Data collected by the AC-9 were interpolated to 1 m depth averages for profile A on June 25, 2000.

These absorption (a) and attenuation (c) measurements were used in a radiative transfer model (HydroLight 4.2, Sequoia Scientific; Mobley, 1994) to calculate spectral light penetration with depth. The wavelengths of interest chosen for the calculations were those of the SeaWiFS sensor, i.e., 412, 443, 490, 510, 540, 555 and 670 nm. The AC-9 wavelengths were interpolated between its sample wavelengths of 412, 440, 488, 510, 532, 555 and 660 to yield Inherent Optical Properties (IOPs) parameters for the calculated wavelengths. Most of the parameter selection was chosen as default values given at the time of installation (number of quads, pure water absorption, etc.). The user specified parameters were selected as follows:

Parameter	Selection
IOP model	User-supplied AC-9 file (ABACBB)
Inelastic scattering	None
Scattering phase function	Constant b_b/b ratio 2.0% (Fornier-Forand)
Wavelength selection	SeaWiFS (see above)
Wind speed	5 m/s
Sky model	RADTRAN
Day of year	176
Time	12:00 pm
Latitude/longitude	29.00°N/89.85°W
Cloud cover	0%
Bottom boundary	Infinitely deep
Output depths	1–30 m (1 m increments)

The time of day and the lack of cloud cover were chosen to maximize downwelling solar irradiance calculations as a best case scenario for photochemical bleaching.

SeaWiFS imagery from June 10, 2000 was obtained from the Naval Research Laboratory–Stennis Space Center, Code 7333 Ocean Sciences Branch, Ocean Optics Section (R. Arnone, personal communication). There was significant cloud cover during the cruise period. The images shown here provide the best view of the Mississippi Plume just prior to the start of the cruise. Fig. 1A shows the absorption at 412 nm by colored particulate and dissolved matter. Fig. 1B shows the scattering by particles at 555 nm. Both images show the plume is constrained to the nearshore with the plume from Southwest Pass proceeding to the

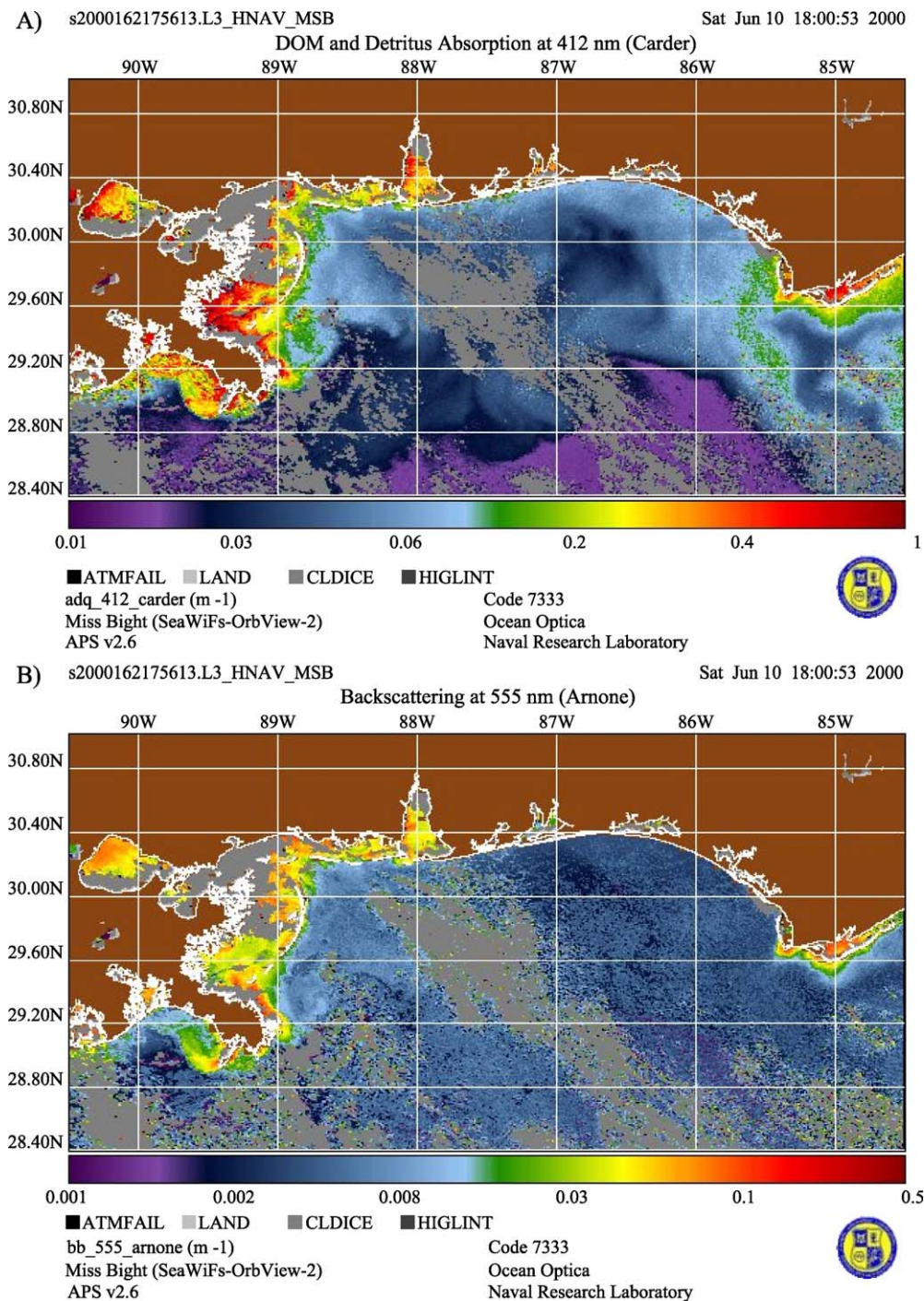


Fig. 1. SeaWiFS imagery from June 10, 2000. Absorption at 412 nm (A) and particle scattering at 555 nm (B). Images courtesy of R. Arnone, Naval Research Laboratory-Stennis Space Center.

west–northwest and the plume on the eastside of the Birdfoot region hugging the coast.

2.10. Flow-field flow fractionation

Flow-field flow fractionation (FIFFF) is a chromatographic-like technique that provides separation of colloidal matter into a size continuum along an open, ribbon shaped channel bounded top and bottom by ceramic frits (Giddings, 1993). Briefly, as colloidal constituents are transported down a $\sim 250 \mu\text{m}$ high $\times 2$ cm wide channel a cross channel flow field is applied to drive colloidal constituents towards the accumulation wall lined with a 1 kDa membrane. This field is opposed by the colloidal diffusivities, with smaller colloids moving further away from the channel wall and into the faster moving along-channel flow lamellae while larger colloids (lower diffusivities) stay closer to the accumulation wall and thus move more slowly along the channel. Measuring the absorbance of the channel outflow provides a measure of colloidal concentrations over time, yielding a “fractogram” of the colloidal size continuum.

A F-1000 FO Universal Fractionator (PostNova Analytics, Salt Lake City, UT) was used for this study after modification for on-channel preconcentration of samples. Briefly, 5 ml samples were focused on-channel and separations done using a channel flow of 2.0 ml min^{-1} and a constant crossflow rate of 4.0 ml min^{-1} for the 30–40 min separation. The carrier solution, used for both focusing and transport of the colloidal concentrates along the channel to the detector, was offshore ultrafiltered (<1 kDa) seawater (Millipore Prep Scale cartridges). A Hyper Quan UV detector was used to measure the absorption at 254 nm in the channel outflow. Full details of the analytical methods are given in Wells (2004; this issue).

3. Results

3.1. High resolution measurements

Continuous, in situ, real-time data allowed the identification of subsurface CDOM maxima that existed in thin layers in specific areas underneath

the Mississippi River Plume. This phenomenon was observed on six separate cross-shelf transects, Lines 12 and 14 on the east side of the Birdfoot region, and Lines 20, 22, 24, 26 on the west side (see Fig. 1A and B in Chen and Gardner, 2004, this issue for maps of these Lines). In all cases, CDOM was high at the surface in the low salinity plume, decreased at the base of the plume as salinity increased, and then increased at the pycnocline without a concurrent change in salinity. The subsurface CDOM maxima were consistently found in conjunction with a density discontinuity, however not all density steps had associated CDOM maxima. These subsurface maxima in CDOM varied in depth from 16 to 29 m. In addition, increasing CDOM with depth in the cold waters beneath the pycnocline suggests an intrusion of a distinct water mass, potentially cold deep water from offshore that has not experienced photobleaching. The real-time data from the ECOShuttle allowed us to precisely sample the thin layer maxima because of the approximate 3 min delay time between in situ measurements and when that water was pumped through the 200 m Teflon tube to our sampling port aboard ship. On Line 22, the ECOShuttle was purposely flown at the depths at which we observed the subsurface CDOM maximum on several passes through the plume (Fig. 2). Table 1 shows the discrete samples taken at the surface and in the subsurface maxima.

Fig. 2 shows the two-dimensional distribution of CDOM on Line 22. Several CDOM maxima in this subsurface region below the plume are seen. A feature at ~ 24 m depth and 23.4 kg/m^3 density is seen as a broad maximum in “A”, a sharp maximum in “C”, and a broader maximum more offshore in “B”. Another feature at ~ 29 m depth and 23.9 kg/m^3 density appears as a sharp maximum in “A” and “B” and no clear maximum in “C”. In all three profiles, it appears that CDOM is high and increasing below 30 m, but consistent observation of this deepest feature is limited by the depth of ECOShuttle flight. Because we were traversing the thin layers vertically as we were moving across the features at 8 knots horizontally, each pass (undulation) does not fall exactly upon the previous one (Fig. 2A, profiles “A”, “B”, and “C”). The inconsistency of the features over such small horizontal distances suggests a somewhat ephemeral nature of the CDOM accumulation, possibly due to

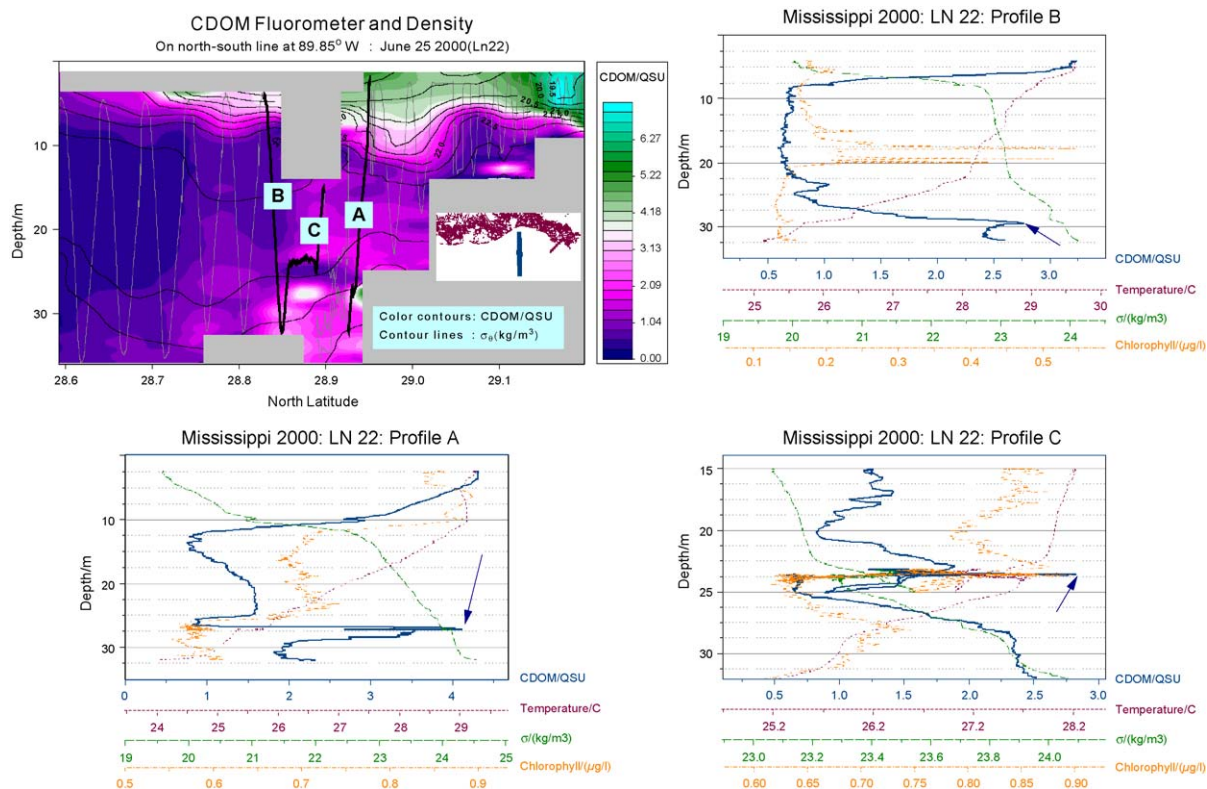


Fig. 2. (A) CDOM distribution along Line 22 in June 2000. Shading shows CDOM concentrations recorded by the SeaTech fluorometer. Drawn contours represent density. (Profiles A, B and C) Depth profiles of individual “undulations” of the ECOShuttle as highlighted in (A) with arrows denoting the subsurface CDOM maxima. Note changes of scale in Profile C.

physical processes, possibly CDOM formation processes. Nonetheless, these high-resolution data show clear steps in density at the depth of the CDOM maxima (e.g. 24 m in Fig. 2: profile C). While maxima in chlorophyll fluorescence sometimes occurred at subsurface CDOM maxima (profile “C” @ 24 m), chlorophyll fluorescence does not generally correlate with CDOM maxima (Fig. 2). For example, in profile “A” at 29 m depth, there is no evidence for an increase in chlorophyll fluorescence associated with this rather large CDOM maximum. By plotting sensor data from the CDOM fluorometer (SeaTech) versus salinity, we see that the production of CDOM, unrelated to any decrease in salinity (river water influence) is apparent in the subsurface layers of CDOM at salinities >36 (Fig. 3).

Similar features were observed on Lines 12, 14, 20, and 24. We assume that the low salinity Mississippi Plume water in the upper 12 m in the area

was all of similar origin (composition) and that subsurface layers of CDOM were of similar origin (composition) in subsequent analyses of the samples (Tables 1 and 2).

3.2. Optical measurements

Excitation–emission matrices (EEMs) of CDOM fluorescence at two depths on Line 20 are clearly different (Fig. 4). In these EEMs, four characteristic peak positions are labeled as previously described by Coble (Coble, 1996). These regions include a primary fluorescence peak from dissolved humic substances (Peak A), a secondary humic substances peak characteristic of terrestrially derived DOM (Peak C), a secondary humic substances peak characteristic of marine-derived DOM (Peak M), and a “protein-associated” peak attributable to fluorescence from aromatic amino acids, primarily tryptophan and/or tyrosine

Table 1
Discrete measurements of surface (plume) and subsurface samples

Sample no.	Line	Comments	Depth (m)	Latitude (°N)	Longitude (°W)	Salinity	Temperature (°C)	CDOM (QSU) ^a	DOC (μM)	Fluorescence (QSU)	α_{337} (m ⁻¹)
77	Line 12	Subsurface Max	18	29.056	88.767	36.03	27.45	1.16	80.9	1.44	0.231
78	Line 12	Plume	2.5	29.019	88.768	33.63	28.99	3.71	88.3	4.99	0.637
79	Line 12	Plume	3.4	28.959	88.769	33.48	28.59	3.69	96.2	3.54	0.456
117	Line 14	Plume	4.76	29.624	88.502	33.64	28.82	5.28	91.7	3.13	0.490
118	Line 14	Subsurface Max 20 m	19.12	29.641	88.501	35.92	24.24	4.84	71.3	2.77	0.483
119	Line 14	Subsurface Min 15 m	15.21	29.666	88.501	35.55	26.21	3.53	69.4	2.17	0.361
120	Line 14	Plume	3.05	29.781	88.499	33.31	28.95	5.95	99.8	3.63	0.436
148	Line 20	Offshore Surface Water	2.81	28.648	89.619	35.95	28.79	0.43	73.0	0.53	0.090
149	Line 20	Subsurface max	29	28.721	89.618	36.15	26	0.57	123.2	4.23	0.616
156	Line 22	Plume	2.76	29.081	89.851	32.58	29.01	4.32	92.3	1.29	0.427
157	Line 22	Plume	3.22	28.963	89.849	31.92	29.11	4.28	123.5	5.22	0.389
158	Line 22	Subsurface Max	16.46	28.896	89.847	36	28.15	1.25	80.2	1.53	0.468
159	Line 22	Plume	4.82	28.788	89.846	32.75	29.66	3.02	103.0	3.89	0.138
187	Line 26	Subsurface Max	29.7	28.415	90.359	36.09	26.06	1.71	76.1	2.08	0.431
188	Line 26	Surface	5.7	28.351	90.359	35.83	28.84	0.48	54.1	0.52	0.065
191	Line 28	Surface	2.21	28.449	90.657	35.84	29.15	0.57	59.4	0.32	0.033

Absorbance measurements were made at 337 nm.

^a CDOM represents the SeaTech CDOM fluorometer on the ECOShuttle measured in (V) converted to QSU by calibrating with discrete samples (Chen and Gardner, 2004).

(Peak T). The EEM spectra of the CDOM in the subsurface layer exhibited an increased relative “protein” peak compared with the surface layer (Fig. 4). The subsurface CDOM had a particularly strong protein fluorescence with comparatively little humic fluorescence (Fig. 4B). The plume CDOM (Fig. 4A) also had significant protein fluorescence in the T region, but the humic fluorescence was considerably stronger than observed with the subsurface CDOM sample.

The Wetlabs AC-9 continuously recorded nine wavelengths from 412 to 750 nm. A thin layer is clearly seen in a plot of Absorption (412 nm) vs. depth for Line 22 (Fig. 5; corresponds to Fig. 2, profile “C”). Absorbance is high in the surface plume, decreases with depth, and apparently increases in the thin layer sitting on the pycnocline. While the AC-9 was measuring unfiltered water and is probably affected in absolute measurements in terms of its absorption coefficient, the measurements on the pumped seawater confirm that a thin layer of material is present at ~ 24 m depth. With only a small increase in optical backscatter (data not shown) at this depth, the AC-9 is most probably responding

to dissolved organic matter. Absorbance is higher below the subsurface thin layer where intrusion from deeper waters offshore brings in more colored water. Additionally, the spectral slope coefficient (Green and Blough, 1994; Blough and Del Vecchio, 2002) in the subsurface maximum seawater (Line 20) is lower than at the surface (Table 3). The higher spectral slope coefficient in the plume may reflect its greater exposure to solar radiation. Other studies have shown that CDOM photobleaching is accompanied by increases in *S* (Blough and Del Vecchio, 2002).

3.3. Light availability

Based on the AC-9 IOP measurements there was very little light available at depth for biological or photochemical reactions. Fig. 6 shows the depth dependent diffuse attenuation coefficient for Profile A (see Fig. 2) for 412 and 555 nm. The large concentration of particulate and dissolved material shifts the peak transparency of this water from ~ 430 nm for pure water (Pope and Fry, 1997; Bissett et al., 2001) to ~ 540 nm (data not shown). The Hydro-

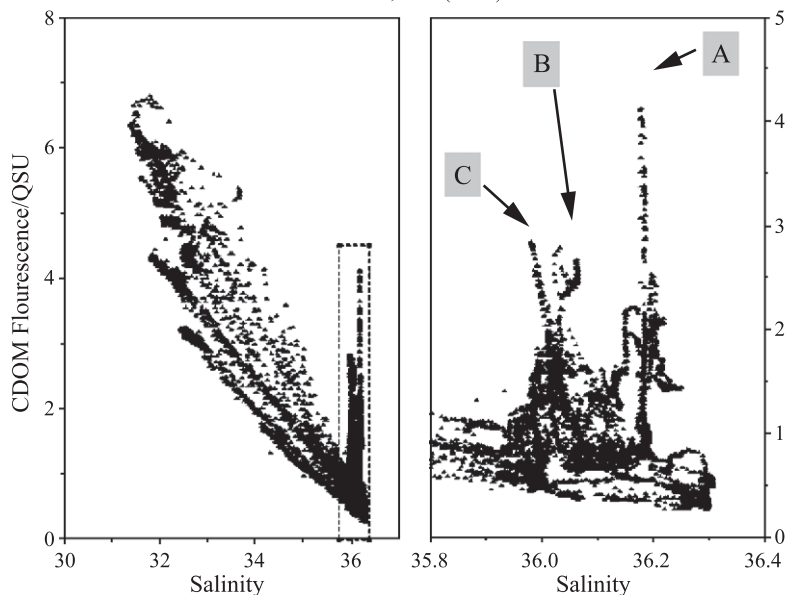
CDOM-Salinity Curve for North-South Line at 89.85°W
June 25, 2000(Ln22)

Fig. 3. CDOM fluorescence vs. salinity for the entire Line 22 transect highlighting the in situ production of CDOM in the subsurface (Profiles A, B, and C are labeled) as well as the three distinct water masses with different apparent freshwater endmembers (Chen and Gardner, 2004, this issue).

light calculations suggest there was little light at depth with only 0.149% and 0.017% of the surface irradiance at 412 nm reaching 14 and 24 m, respectively. These values increase for the light at 555 nm to 2.816% and 0.541% of surface irradiance at 15 and 24 m, respectively.

As the sunlight-normalized action spectra of CDOM photolysis is maximal around 300 nm (Kieber et al., 1990), and the spectral slope coefficient of the CDOM absorption is 0.018–0.021 (Table 3), it is clear that there is virtually no photochemically active light at depth. Biologically active light,

however, would depend on the photosynthetic action spectra of the cells dominating the chlorophyll *a* biomass peak. At the clear sky irradiance level used in this calculation, approximately $50 \mu\text{Ein m}^{-2} \text{s}^{-1}$ reaches 15 m, and $\sim 9 \mu\text{Ein m}^{-2} \text{s}^{-1}$ reaches 24 m, dominated by light in the middle 500 nm range, sufficient for low-levels of photosynthesis. However, as is evident from the satellite images (Fig. 1A and B), clear skies were not the norm during the cruise. It is unclear how much photosynthesis was possible, but the possibility that some small amount was occurring cannot be excluded.

Table 2
Discrete samples taken for bioassay and irradiation studies

Sample	Line	Sample no.	Depth (m)	Latitude	Longitude	CDOM fluorescence (QSU)
Experiment 1 subsurface	12	77	18	29 03 188	88 46 052	1.16
Experiment 1 surface	12	78	2.3	29 01 616	88 76 800	3.71
Experiment 2 subsurface	20	149	29	28 43 279	89 37 089	0.57
Experiment 2 surface	20	148	1	28 45 532	89 37 065	0.43
Experiment 3 subsurface	26	187	29.6	28 25 323	90 21 550	1.71
Experiment 3 surface	28	191	2	28 37 714	90 39 340	0.57

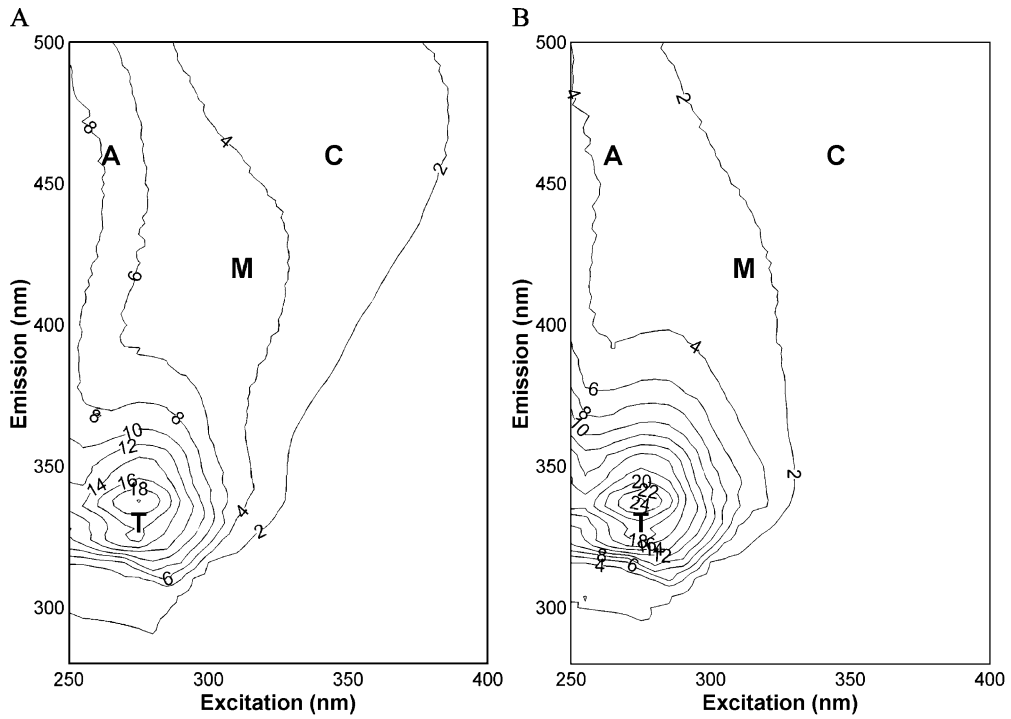


Fig. 4. Excitation–emission matrices of the surface (A) and subsurface (B) CDOM maxima on Line 20. Note the relatively higher protein fluorescence in the subsurface sample. The locations of Peaks A, C, M, and T (Coble, 1996) are included.

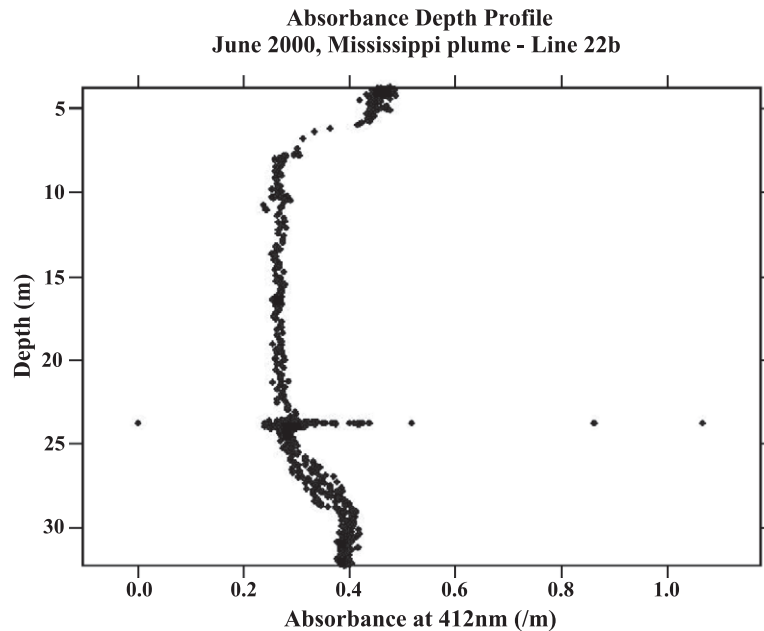


Fig. 5. AC-9 absorption at 412 nm vs. depth for Line 22 (Corresponds to Fig. 2, Profile “C”) in the vicinity of the subsurface maximum.

Table 3

Effects of solar irradiation on the biological and photochemical degradation of surface (plume) and subsurface samples described in Table 2

Sample	Normalized respiration, Dark	Normalized respiration, Irradiated	Photoinduced change in normalized respiration (%)	S, Dark	S, Irradiated	Photoinduced change in α_{350} (%)	Photoinduced change in EEM humic region (%)
Experiment 1 subsurface	11.5 ± 2.5	14.1 ± 3.6	+ 22.6	0.0185	0.0181	− 2.6 ± 0.3	− 24.2
Experiment 1 surface	11.0 ± 0.66	11.9 ± 1.8	+ 8.2	0.0182	0.0203	− 19.7 ± 2.0	− 23.5
Experiment 2 subsurface	11.2 ± 9.0	13.4 ± 6.0	+ 19.6	0.0171	0.0168	− 12.4 ± 1.0	− 12.3
Experiment 2 surface	2.6 ± 3.0	12.6 ± 5.4	+ 385	0.0207	0.0207	− 6.9 ± 0.7	− 4.5
Experiment 3 subsurface	8.45 ± 4.7	10.4 ± 1.3	+ 23.1	0.0200	0.0181	+ 13.0 ± 1.3	n.a.
Experiment 3 surface	0.17 ± 2.2	5.58 ± 6.3	+ 3180	0.0219	0.0222	− 3.1 ± 0.4	n.a.

The term α_{350} denotes the absorption coefficient at 350 nm.

3.4. Biological and photochemical reactivity and biologically available photoproducts

Experiments were conducted to compare the biological and photochemical reactivity of the surface and subsurface CDOM maxima, and to determine rates of formation of biologically labile photoproducts from the two CDOM layers (Table 3). In two of three experiments (Experiment 2, Line 20; Experi-

ment 3, Lines 26/28; Table 2), the subsurface CDOM layer was found to be more susceptible to biological degradation but produced fewer biologically labile photoproducts relative to the surface CDOM layer. In Experiment 2, bacterial respiration of subsurface DOM (normalized to DOC concentration) averaged 11.2 $\mu\text{M O}_2/\text{mg C}$ ($n=3$) over a 2-week incubation, compared to an average of 2.6 $\mu\text{M O}_2/\text{mg C}$ for the surface DOM (Table 3). Likewise, in Experiment 3, subsurface DOM was more susceptible to biological degradation than surface DOM (averages of 8.5 vs. 0.2 $\mu\text{M O}_2/\text{mg C}$ over a 2-week incubation; $n=3$). In contrast, release of biologically labile photoproducts was lower for the subsurface CDOM than for the surface CDOM. In Experiment 2, bacterial respiration of subsurface DOM averaged an additional 2.2 $\mu\text{M O}_2/\text{mg C}$ as a result of irradiation with simulated natural sunlight for 4 h prior to the 2-week microbial respiration assay, compared to an average of 10.0 $\mu\text{M O}_2/\text{mg C}$ for the surface (Table 3). In Experiment 3, subsurface CDOM similarly yielded fewer biologically labile photoproducts than surface CDOM (2.0 vs. 5.5 $\mu\text{M O}_2/\text{mg C}$; $n=3$). In a third experiment (Experiment 1, Line 12), we found no significant difference in rates of bacterial degradation of surface and subsurface samples, and neither produced measurable biologically labile photoproducts.

The effects of irradiation on the optical properties of the subsurface and surface CDOM were also

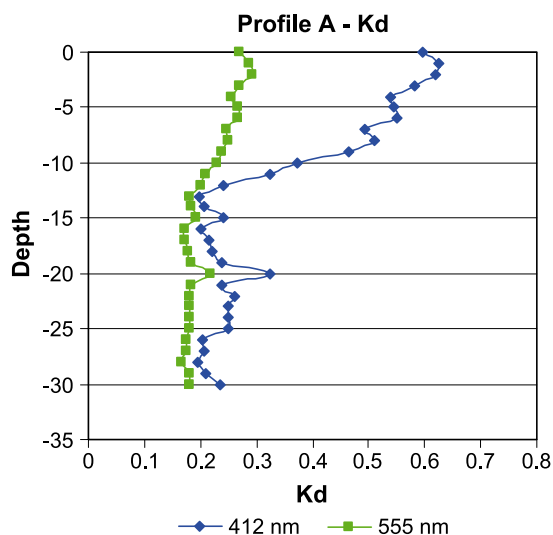


Fig. 6. Calculated K_d vs. depth for Profile A (Fig. 2). K_d s are shown for 412 and 555 nm and are calculated from AC-9 data as described in the text.

examined in the three experiments (Table 3). Averaged over all the studies of photoinduced changes in absorption coefficients, the subsurface CDOM was less photoreactive than the surface CDOM. The exception was the subsurface CDOM in Experiment 2, however, which photobleached somewhat more rapidly than the surface CDOM (Table 3). The effects of irradiation on the spectral slope coefficients differed between the subsurface and surface material. Irradiation generally caused a decrease in the spectral slope coefficients for the subsurface CDOM but photoreaction had the opposite effect on the surface CDOM. Photoinduced changes in the humic region of the fluorescence EEMs was more complex. Generally, the fluorescence of both the subsurface and surface CDOM bleached on irradiation and the decrease was similar in magnitude to that observed for the absorption coefficients (350 nm) (Table 3).

3.5. Field flow-fractionation (FIFFF)

The FIFFF analyses of colloidal matter show distinct differences in colloidal CDOM size distribution among surface waters directly influenced by the Mississippi plume (Fig. 7A), a subsurface CDOM maximum that coincided with a chlorophyll maximum (Fig. 2: profile C; Fig. 7B), and water from a deep chlorophyll maximum from offshore waters (no CDOM maximum; Fig. 7C; Wells, 2004, this issue). Increasing retention times represent larger sized particles/colloids. Clearly, the two peaks that are present in the surface sample are not reproduced in the subsurface CDOM maximum thin layer sample. This subsurface peak shows a single peak of small material and a slight indication of some very large material. The subsurface CDOM maximum sample also showed little similarity to a classic deep chlorophyll maximum observed in offshore waters (blue waters offshore of the plume) where only a single larger material peak was present. These fractogram absorbances were measured at 254 nm (i.e., below the wavelengths normally used to define CDOM) due to limited sensitivity of measurements at higher wavelengths. A small subset of nearshore (high CDOM) samples measured at both 254 and 290 nm yielded very similar fractogram patterns. It is important to recognize nonetheless that these changes in FIFFF may not exactly reflect fluctuations in colloidal

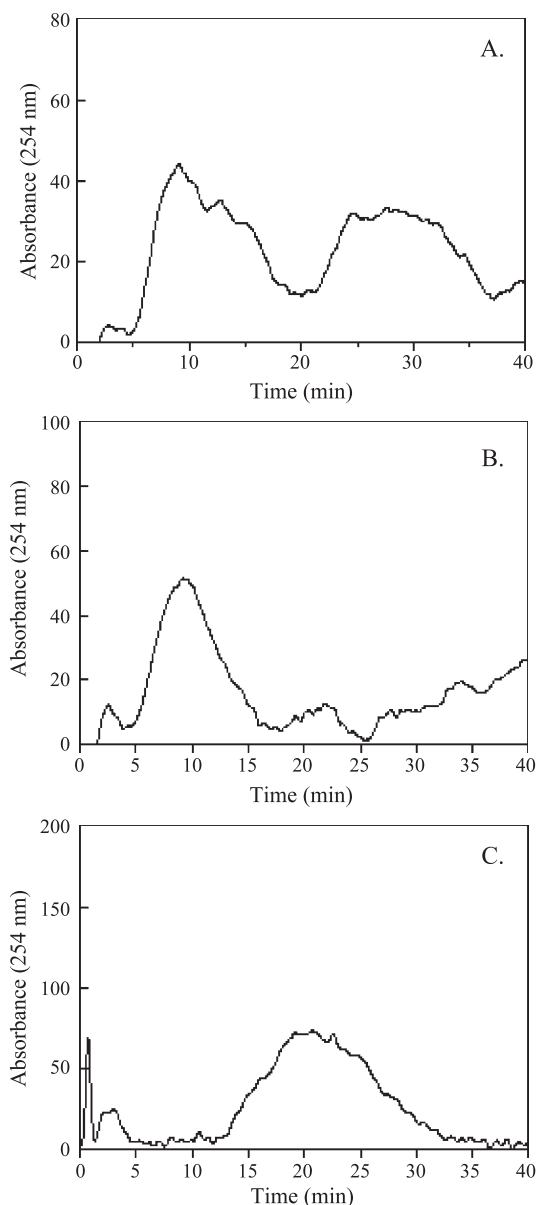


Fig. 7. Field flow-fractionation fractograms of surface (A), subsurface CDOM maximum (B), and deep chlorophyll maximum (C) samples. Sample in (A) is similar to discrete sample #157, ~ 3 m depth (samples were taken on pumped water immediately following #157). Sample in (B) is similar to discrete sample #158 at ~ 16 m depth. Sample in (C) was taken from a CTD hydrocast at 28°20.71'N, 90°21.24'W at 47 m depth. Bottom depth was 58 m. Longer retention times correlate with higher molecular weights (see Wells, 2004, this issue, for details).

CDOM measured at higher (300–400 nm) wavelengths. With this caveat then, the different CDOM size distributions at the surface, in the subsurface thin layers below the plume, and at the deep chlorophyll maxima likely suggests that these materials have a different source and perhaps composition.

3.6. Stable carbon isotopes

DOC concentrations were not noticeably higher ($<2 \mu\text{M}$ difference) in subsurface maxima and minima of CDOM (Table 1). This implies that total carbon represented by the increased CDOM in the subsurface layer is small ($<3\%$ of the total DOC). The small quantitative increase in DOC is also supported by the fact that stable carbon isotopes of subsurface maxima samples (DOC $\delta^{13}\text{C} = -21.9\%$ to -22.1%) were slightly higher but not significantly different from surface water values (DOC $\delta^{13}\text{C} = -22.5\%$ to -23.1%) considering that the surface DOC was more affected by the Mississippi River fresh water discharge in the region (Wang et al., 2004, this issue). Apparently, the different nature of the CDOM in the two layers did not significantly affect the total concentration (Nelson et al., 1998) or stable isotope ratio of the DOC in the two layers.

4. Discussion

We propose that subsurface CDOM layer observed in the Gulf of Mexico in June 2000 was produced by bacterial reworking of phytoplankton-derived organic matter, and was distinct in origin, composition, and cycling from the surface CDOM associated with the Mississippi River plume. Evidence for in situ origin of the subsurface layer includes: (1) Subsurface CDOM maxima were not associated with low salinity water; (2) Optical properties relating to absorbance and fluorescence characteristics differed considerably and consistently between surface and subsurface maxima; (3) Biological and photochemical reactivity differed between the two CDOM pools, with evidence for rapid photochemical but slow biological cycling of surface CDOM and rapid biological but slow photochemical cycling for subsurface CDOM; (4) The size spectrum of colloidal particles differed for the surface and subsurface CDOM pools, and was

consistent with detrital origin for the subsurface CDOM (see Wells et al., 2004, this issue).

CDOM produced through the decay of algal detritus has been referred to as “microbially derived” (McKnight et al., 1994, 2000). In contrast, the terrestrially derived CDOM present in the plume waters is presumed to originate largely through the decomposition of vascular plant material in soils and sediments. Differences between the optical and physicochemical properties of these distinct CDOM types are related to the molecular properties, and have been discussed previously (Thurman, 1985; Chin et al., 1994; McKnight et al., 1994, 2000; Blough and Green, 1995; Blough and Del Vecchio, 2002). For example, CDOM in the open ocean has a significantly lower aromatic content and $a(\lambda)^*$ coefficients than terrestrially derived CDOM (Blough and Del Vecchio, 2002) that can be ascribed to the chemical composition of the source material. In the present study, CDOM of microbial and terrestrial origin appeared to be present simultaneously in a system, but distinguishable based on chemical, optical, and biological properties.

Although direct production of CDOM from living phytoplankton is another potential source of the subsurface CDOM layer, evidence points more strongly to bacterial decomposition of phytoplankton cells. Correlations of CDOM with chlorophyll *a* were not consistent during this study, suggesting a decoupling of phytoplankton biomass from the amount of CDOM production (Nelson et al., 1998). The Hydro-light model indicates that very little, if any, photosynthetically active light reached the level of the CDOM maximum (pycnocline ~ 24 m) during this cruise, suggesting that phytoplankton cells observed in association with the pycnocline were not active. In a previous study, indirect formation via bacterial reworking of phytoplankton biomass, rather than direct formation from living algae, was found to be the source of CDOM in algal cultures (Rochelle-Newall and Fisher, 2002b). Thus it is more likely that bacteria were concentrated on the pycnocline and reworking colorless detrital material (dissolved or particulate) derived from particles above or from slow growth at depth.

Using a mass balance approach, Chen et al. (2002) showed that in situ production of CDOM dominates over riverine inputs when a large shelf-wide study area

is considered. Because of the calm conditions experienced in the northern Gulf of Mexico during June 2000, CDOM accumulation associated with stable pycnoclines could be observed. It is likely that in situ bacterially mediated CDOM production is consistently important in this system, but strong mixing and lack of stable pycnoclines usually preclude accumulation of CDOM into an observable layer. Bacterially mediated CDOM production and riverine CDOM also change seasonally, so the relative amounts of each source can change seasonally. However, Chen and Gardner (2004, this issue) use non-conservative mixing lines of CDOM vs. salinity to provide evidence of ubiquitous in situ production of CDOM in both summer and spring. The amount of carbon involved in this process may be small (a few percent), but the total amount of CDOM produced may be quite significant. It is estimated that due to the ubiquitous nature of this source at all depths, the in situ biological production mechanism is the dominant source of CDOM in the northern Gulf of Mexico below the upper 12 m (Chen and Gardner, 2004, this issue).

Exposure to solar radiation can potentially affect CDOM transformations through photochemical modification of its biological availability (Moran and Zepp, 1997, 2000; Zepp et al., 1998; Miller, 1999; Miller et al., 2002; Zepp, 2002). This effect is well documented in the case of terrestrially derived DOC, where stimulation of microbial degradation of CDOM is usually observed. However, the relative importance of this pathway seems to strongly depend on the DOC source, and may not be effective for microbially derived CDOM. Microbial degradation of surface water DOM in the open ocean (Benner and Biddanda, 1998; Obernosterer et al., 1999) and a subtropical seagrass meadow (Ziegler and Benner, 2000) was not stimulated by solar irradiation. Photoreactions can reduce the microbial availability of certain organic substrates such as peptone and algal exudates (Thomas and Lara, 1995; Naganuma et al., 1996; Tranvik and Kokalj, 1998), possibly via light-induced cross-linking between the CDOM and algal exudates (Tranvik and Kokalj, 1998). Our study showed low photochemical reactivity and little formation of biologically labile photoproducts from the subsurface CDOM layer proposed to be of microbial origin. In contrast, microbial decomposition of surface CDOM in the Mississippi River plume was measurably stimulated by exposure to

sunlight. These data suggest significantly different turnover times by biological and photochemical processes for marine CDOM pools of differing origins.

Acknowledgements

This research was supported by grants from the Office of Naval Research to RFC (N00014-00-1-0325), MW (N00014-00-1-0304), PC (N00014-01-0041), MAM (N00014-98-1-0530) and RGZ (N00014-98-F-0202) and WPB (N00014-00-1-01411). We would also like to thank R. Arnone and the Ocean Sciences Branch for the use of the APS processing system of SeaWiFS data during the cruise. This paper has been reviewed in accordance with the U.S. Environmental Protection Agency's peer and administrative review policies and approved for publication. Mention of trade names or commercial products does not constitute an endorsement or recommendation for use by the U.S. EPA.

References

- Babin, M., Stramski, D., 2002. Light absorption by aquatic particles in the near-infrared spectral region. *Limnol. Oceanogr.* 47, 911–915.
- Benner, R., Biddanda, B., 1998. Photochemical transformations of surface and deep marine dissolved organic matter: effects on bacterial growth. *Limnol. Oceanogr.* 43, 1373–1378.
- Bissett, W.P., Schofield, O., Mobley, C., Crowley, M.F., Moline, M.A., 2001a. Methods in microbiology. Paul, J.H. (Ed.), *Marine Microbiology*, vol. 30. Academic Press, London.
- Bissett, W.P., Schofield, O., Glenn, S., Cullen, J.J., Miller, W., Pluddeman, A., Mobley, C., 2001b. Resolving the impacts and feedbacks of ocean optics on upper ocean ecology. *Oceanography* 14, 30–53.
- Blough, N.V., Del Vecchio, R., 2002. Distribution and dynamics of chromophoric dissolved organic matter (CDOM) in the coastal environment. In: Hansell, D., Carlson, C. (Eds.), *Biogeochemistry of Marine Dissolved Organic Matter*. Academic Press, San Diego, CA, pp. 509–546.
- Blough, N.V., Green, S.A., 1995. Spectroscopic characterization and remote sensing of nonliving organic matter. In: Zepp, R.G., Sonntag, C. (Eds.), *The Dahlem Conf. Rept.—The Role of Nonliving Organic Matter in the Earth's Carbon Cycle*. Wiley, Chichester, pp. 23–45.
- Burdige, D.J., Berelson, W.M., Coale, K.H., McManus, J., Johnson, K.S., 1999. Fluxes of dissolved organic carbon from California continental margin sediments—A review. *Geochim. Cosmochim. Acta* 63, 1507–1515.

- Chen, R.F., 1999. In situ fluorescence measurements in coastal waters. *Org. Geochem.* 30, 397–409.
- Chen, R.F., Bada, J.L., 1989. Seawater and porewater fluorescence in the Santa Barbara Basin. *Geophys. Res. Lett.* 16, 687–690.
- Chen, R.F., Bada, J.L., 1992. The fluorescence of dissolved organic matter in seawater. *Mar. Chem.* 37, 191–221.
- Chen, R.F., Gardner, G.B., 2004. High-resolution measurements of chromophoric dissolved organic matter in the Mississippi and Atchafalaya River plume regions. *Mar. Chem.* 89, 105–127 (this issue).
- Chen, R.F., Zhang, Y., Vlahos, P., Rudnick, S.M., 2002. The fluorescence of dissolved organic matter in the Mid-Atlantic Bight. *Deep-Sea Res.*, II 49, 4439–4459.
- Chin, Y., Aiken, G.R., O'Loughlin, E., 1994. Molecular weight, polydispersity, and spectroscopic properties of aquatic humic substances. *Environ. Sci. Technol.* 28, 1853–1858.
- Coble, P.G., 1996. Characterization of marine and terrestrial DOM in seawater using excitation–emission matrix spectroscopy. *Mar. Chem.* 51, 325–346.
- DeGrandpre, M.D., Vodacek, A., Nelson, R.K., Bruce, E.J., Blough, N.V., 1996. Seasonal seawater optical properties of the U.S. Middle Atlantic Bight. *J. Geophys. Res.* 101, 22727–22736.
- Del Castillo, C.E., Coble, P.G., Morell, J.M., Lopez, J.M., Corredor, J.E., 1999. Analysis of the optical properties of the Orinoco River plume by absorption and fluorescence spectroscopy. *Mar. Chem.* 66, 35–51.
- De Souza Sierra, M.M., Donard, O.F.X., Lamotte, M., Belin, C., Ewald, M., 1994. Fluorescence spectroscopy of coastal and marine waters. *Mar. Chem.* 47, 127–144.
- De Souza Sierra, M.M., Donard, O.F.X., Lamotte, M., 1997. Spectral identification and behaviour of dissolved organic fluorescent material during estuarine mixing processes. *Mar. Chem.* 58, 51–58.
- Giddings, J.C., 1993. Field-flow fractionation; analysis of macromolecular, colloidal, and particulate materials. *Science* 260, 1456–1465.
- Green, S.A., Blough, N.V., 1994. Optical absorption and fluorescence properties of chromophoric dissolved organic matter in natural waters. *Limnol. Oceanogr.* 39, 1903–1916.
- Hayase, K., Shinozuka, N., 1995. Vertical distribution of fluorescent organic matter along with AOU and nutrients in the equatorial Central Pacific. *Mar. Chem.* 48, 283–290.
- Hayase, K., Tsubota, H., Sunada, I., Goda, H., Yamazaki, H., 1988. Vertical distribution of fluorescent organic matter in the North Pacific. *Mar. Chem.* 25, 373–381.
- Kieber, R.J., Zhou, X., Mopper, K., 1990. Formation of carbonyl compounds from UV-induced photodegradation of humic substances in natural waters: fate of riverine carbon in the sea. *Limnol. Oceanogr.* 35, 1503–1515.
- McKnight, D.M., Andrews, E.D., Spaulding, S.A., Aiken, G.R., 1994. Aquatic fulvic acids in algal-rich Antarctic ponds. *Limnol. Oceanogr.* 39, 1972–1979.
- McKnight, D.M., et al., 2000. Spectrofluorometric characterization of dissolved organic matter for indicator of precursor organic material and aromaticity. *Limnol. Oceanogr.* 46, 38–48.
- Meyers-Schulte, K.J., Hedges, J.I., 1986. Molecular evidence for a terrestrial component of organic matter dissolved in seawater. *Nature* 321, 61–63.
- Miller, W.L., 1999. Effects of UV radiation on aquatic humus: photochemical principles and experimental considerations. In: Hessen, D.O., Tranvik, L. (Eds.), *Aquatic Humic Substances*. Springer-Verlag, New York, pp. 125–143.
- Miller, W.L., Moran, M.A., Sheldon, W.M., Zepp, R.G., Opsahl, S., 2002. Determination of apparent quantum yield spectra for the formation of biologically labile photoproducts. *Limnol. Oceanogr.* 47 (2), 343–352.
- Mobley, C.D., 1994. *Light and Water*. Academic Press, San Diego, CA.
- Moran, M.A., Zepp, R.G., 1997. Role of photoreactions in the formation of biologically labile compounds from dissolved organic matter. *Limnol. Oceanogr.* 42, 1307–1316.
- Moran, M.A., Zepp, R.G., 2000. UV radiation effects on microbes and microbial processes. In: Kirchman, D. (Ed.), *Microbial Ecology of the Oceans*. Wiley, New York, pp. 201–228.
- Morris, D.P., Hargreaves, B.R., 1997. The role of photochemical degradation of dissolved organic matter in regulating UV transparency of three lakes on the Pocono Plateau. *Limnol. Oceanogr.* 42, 239–249.
- Naganuma, T., Konishi, T., Inoue, T., Nakane, T., Sukizaki, S., 1996. Photodegradation or photoalteration? Microbial assay of dissolved organic matter. *Mar. Ecol., Prog. Ser.* 135, 309–310.
- Nelson, N.B., Siegel, D.A., Michaels, A.F., 1998. Seasonal dynamics of colored dissolved organic material in the Sargasso Sea. *Deep-Sea Res.*, I 45, 931–957.
- Obernosterer, I., Reitner, B., Herndl, G.J., 1999. Contrasting effects of solar radiation on dissolved organic matter and its bioavailability to marine bacterioplankton. *Limnol. Oceanogr.* 44, 1645–1654.
- Opsahl, S., Benner, R., 1997. Distribution and cycling of terrigenous dissolved organic matter in the ocean. *Nature* 386, 480–482.
- Pope, R.M., Fry, E.S., 1997. Absorption spectrum (380–700 nm) of pure water. II. Integrating cavity measurements. *Appl. Opt.* 36, 8710–8723.
- Rochelle-Newall, E.J., Fisher, T.R., 2002a. Chromophoric dissolved organic matter and dissolved organic carbon in Chesapeake Bay. *Mar. Chem.* 77, 23–41.
- Rochelle-Newall, E.J., Fisher, T.R., 2002b. Production of chromophoric dissolved organic matter fluorescence in marine and estuarine environments: an investigation into the role of phytoplankton. *Mar. Chem.* 77, 7–21.
- Rochelle-Newall, E.J., Fisher, T.R., Fan, C., Glibert, P.M., 1999. Dynamics of chromophoric dissolved organic matter and dissolved organic carbon in experimental mesocosms. *Int. J. Remote Sens.* 20, 627–641.
- Skoog, A., Hall, P.O.J., Hulth, S., Paxeus, N., van der Loeff, M.R., Westerlund, S., 1996. Early diagenetic production and sediment–water exchange of fluorescent dissolved organic matter in the coastal environment. *Geochim. Cosmochim. Acta* 60, 3421–3431.
- Thomas, D.N., Lara, R.J., 1995. Photodegradation of algal derived dissolved organic carbon. *Mar. Ecol., Prog. Ser.* 116, 309–310.

- Thurman, E.M., 1985. *Organic Geochemistry of Natural Waters*. Nijhoff/Junk, Boston. 97 pp.
- Tranvik, L.J., Kokalj, S., 1998. Decreased biodegradability of algal DOC due to interactive effects of UV radiation and humic matter. *Aquat. Microb. Ecol.* 14, 301–307.
- Twardowsky, M., Donaghay, P., 2001. Separating in situ and terrigenous sources of absorption by dissolved materials in coastal waters. *J. Geophys. Res.* 106, 2545–2560.
- Urban-Rich, J., 1999. Release of dissolved organic carbon from copepod fecal pellets in the Greenland Sea. *J. Exp. Mar. Biol. Ecol.* 232, 107–124.
- Vlahos, P., Chen, R.F., Repeta, D.J., 2002. Fluxes of dissolved organic carbon (DOC) in the Mid-Atlantic Bight. *Deep-Sea Res., II* 49, 4369–4385.
- Wang, X.-C., Chen, R.F., Gardner, G.B., 2004. Organic matter cycling in the Mississippi River plume. *Marine Chemistry* (this issue).
- Wells, M.L., 2004. Field flow-field fractionation of organic matter in the Mississippi Plume region. *Mar. Chem.* (this issue).
- Zepp, R.G., 2002. Solar ultraviolet radiation and aquatic carbon, nitrogen, sulfur and metals cycles. In: Helbling, E.W., Zagarese, H. (Eds.), *UV Effects in Aquatic Organisms and Ecosystems*. Royal Society of Chemistry, Cambridge, UK, pp. 137–183.
- Zepp, R.G., Callaghan, T.V., Erickson, D.J., 1998. Effects of enhanced solar ultraviolet radiation on biogeochemical cycles. *J. Photochem. Photobiol., B Biol.* 46, 69–82.
- Zepp, R.G., Sheldon, W.M., Moran, M.A., 2004. Dissolved organic fluorophores in southeastern U.S. coastal waters: correction method for eliminating Rayleigh and Raman scattering peaks in excitation–emission matrices. *Mar. Chem.* 189, 15–37 (this issue).
- Ziegler, S., Benner, R., 2000. Effects of solar radiation on dissolved organic matter in a subtropical seagrass meadow. *Limnol. Oceanogr.* 45, 257–266.